

SCIENTIFIC REPORTS



OPEN

Thin-film metallic glass: an effective diffusion barrier for Se-doped AgSbTe₂ thermoelectric modules

Received: 18 November 2016
Accepted: 20 February 2017
Published: 22 March 2017

Chia-Chi Yu¹, Hsin-jay Wu², Ping-Yuan Deng², Matthias T. Agne³, G. Jeffrey Snyder³ & Jinn P. Chu¹

The thermal stability of joints in thermoelectric (TE) modules, which are degraded during interdiffusion between the TE material and the contacting metal, needs to be addressed in order to utilize TE technology for competitive, sustainable energy applications. Herein, we deposit a 200 nm-thick Zr-based thin-film metallic glass (TFMG), which acts as an effective diffusion barrier layer with low electrical contact resistivity, on a high- zT Se-doped AgSbTe₂ substrate. The reaction couples structured with TFMG/TE are annealed at 673 K for 8–360 hours and analyzed by electron microscopy. No observable IMCs (intermetallic compounds) are formed at the TFMG/TE interface, suggesting the effective inhibition of atomic diffusion that may be attributed to the grain-boundary-free structure of TFMG. The minor amount of Se acts as a tracer species, and a homogeneous Se-rich region is found nearing the TFMG/TE interface, which guarantees satisfactory bonding at the joint. The diffusion of Se, which has the smallest atomic volume of all the elements from the TE substrate, is found to follow Fick's second law. The calculated diffusivity (D) of Se in TFMG falls in the range of $D \sim 10^{-20} \sim 10^{-23} (\text{m}^2/\text{s})$, which is $10^6 \sim 10^7$ and $10^{12} \sim 10^{13}$ times smaller than those of Ni [$10^{-14} \sim 10^{-17} (\text{m}^2/\text{s})$] and Cu [$10^{-8} \sim 10^{-11} (\text{m}^2/\text{s})$] in Bi₂Te₃, respectively.

Thermoelectric (TE) materials and modules, which feature the capability of converting waste heat into electricity through the solid-state Seebeck effect, have offered a prospective path to preserve natural resources and to further technological development^{1–3}. The thermal-to-electrical conversion efficiency of TE materials is related to the dimensionless figure-of-merit, $zT = (S^2/\rho\kappa)T$, where S is the Seebeck coefficient, ρ represents the electrical resistivity and κ stands for the thermal conductivity.

In general, the reduction of κ , which may be achieved by introducing nanoparticles/precipitates in the grains or along the grain boundaries^{4–6}, and enhancement of the power factor ($\text{PF} = S^2/\rho$), which might be realized by optimizing the carrier concentration via doping⁷, could lead to higher zT . Despite the large amount of effort to improve zT , the utilization of TE modules as a cost-effective and high-efficiency technology has yet to be realized. In working towards this goal, the thermal stability and mechanical strength of the various joints in TE modules, which typically undergo large thermal fluctuations, is likely to be one of the key issues^{8–13}.

For example, state-of-the-art p -type (Bi, Sb)₂Te₃-based materials, which exhibit zT above unity near room temperature¹⁴, can be joined to metallic electrodes using Sn-based solders such as Bi-Sn or Sn₃Ag_{0.5}Cu solder¹⁵. However, due to the low-melting-point of the solder alloy, the TE modules are limited to low operating temperatures. Alternatively, a solid-liquid interdiffusion bond that results from the incorporation of low-melting point metals/alloys, such as Sn-based or In-based thin films which act as a liquid transient layer¹⁶, is likely to improve the thermal stability and bonding strength of the joints through the formation of high-temperature intermetallic compounds (IMCs) in-between the electrodes and TE materials. However, concerns have been raised about whether the IMCs in multi-layer interdiffusion bonds would be electrically conductive and exhibit a coefficient of thermal expansion (CTE) similar to the other low-temperature liquid transient layers, the TE materials and the electrodes¹⁷. Therefore, in order to obtain the maximum electrical power output and module efficiency, a

¹Department of Materials Science and Engineering, National Taiwan University of Science and Technology, Taipei 10607, Taiwan. ²Department of Materials and Optoelectronic science, National Sun Yat-sen University, Kaohsiung 80424, Taiwan. ³Department of Materials Science and Engineering, Northwestern University, Evanston, IL 60208, USA. Correspondence and requests for materials should be addressed to H.-j.W. (email: ssky0211@mail.nsysu.edu.tw) or J.P.C. (email: jpchu@mail.ntust.edu.tw)

diffusion barrier layer having thin thickness, high thermal stability, and good structural/chemical compatibility with adjacent materials will ensure low electrical and thermal contact resistances at the joint.

For TE modules that operate at temperatures higher than 600 K, the technique of brazing, which introduces a high-melting-point filler metal, is viewed as a possible bonding method, assuming that the thermal stresses accumulated from high-temperature operation and cracking at the brazing joints can be avoided¹⁸. Consequently, the search for adequate diffusion barrier layers is essential for the above-mentioned bonding methods, in order to inhibit the serious inter-diffusion in-between the solder alloys/filler metals and TE materials. Several studies of the interfacial evolutions of TE/metal joints suggest that although the crystalline metals, such as Ni¹⁹, Ti^{20–22} or Mo¹⁹, may seem promising candidates for diffusion barrier layers, their failure is inevitable inside the diffusion barrier layer or at the interface with IMCs after long-term and high-temperature aging^{20,23}. Taking the CoSb₃/(Ni, Mo) joints as an example, instead of blocking the interdiffusion between the solder and TE, the Ni diffusion barrier layer dissolves into the solder. Thermal cycling of CoSb₃/Mo joints results in a fractured interface due to the large CTE mismatch¹⁹.

Herein, a Zr-based thin-film metallic glass (TFMG) is proposed as an alternative diffusion barrier layer for use in mid-temperature TE modules. For this investigation, Se-doped AgSbTe₂, which exhibits a high zT of 1.4 at ≈ 673 K²⁴, is selected as the TE substrate. The diffusion across the TFMG/TE (Se-doped AgSbTe₂) interface is evaluated during thermal aging. Due to the lack of a periodic atomic packing structure, TFMG possess superior mechanical properties compared to their crystalline counterparts²⁵. Moreover, the grain boundaries and/or crystalline defects in crystalline materials can act as diffusive paths for atoms during thermal annealing. TFMGs, however, exhibit high structural disorder and a grain boundary-free structure, leading to their success as diffusion barriers in copper metallization²⁶, CIGS solar cells²⁷ and tin whisker mitigation of microelectronic packaging²⁸, despite the short-term annealing of these systems. As a result of having an amorphous structure, the thermal conductivity of ZrCuAlNi metallic glass, reported to be ~ 5 W/mK at 300 K²⁹, is lower than that of typical metallic electrodes (e.g. Ni and Ti, $\kappa > 20$ W/mK at 300 K). Nevertheless, the influence of thermal resistance of TFMG can be ignored due to the thin thickness (~ 200 nm) of TFMG (compared to mm-thick TE leg).

In order to evaluate the feasibility of TFMG as a diffusion barrier, a 200-nm-thick ZrCuAlNi TFMG layer is deposited on one side of the Ag₂₅Sb₂₅Se₅Te₄₅ (TE substrate), while a crystalline Ni layer with the same thickness is deposited on the other side of the TE substrate, to form a sandwich-like structure of TFMG (200 nm)/TE substrate/Ni (200 nm). After thermal aging from 8 to 360 h at 673 K, the Se atom, originating from the TE substrate, diffuses into the TFMG and forms a homogeneous Se-rich region nearing the TFMG/TE interface, which ensures satisfactory bonding at the joint. Furthermore, no IMCs are found at the interface between the TFMG and TE substrate, reducing the possibility of high electrical contact resistance and low ductility that is commonly observed in electronic packages³⁰. For example, the electrical resistivity has been observed to increase with the annealing time in Cu/Sn-3Cu/Cu reaction couples³⁰, mainly attributed to the increasing thickness of the IMC reaction layer.

Contrary to the TFMG/TE result, the diffusion couple of Ni/TE reveals extensive formation of Ni-Te-Sb IMCs and voids even after comparably short-term annealing. This suggests that the amorphous thin film, which provides less channels for diffusion than that of a (poly)crystalline one, might be appropriate for use as a diffusion barrier layer in mid-temperature TE modules.

Results and Discussion

The thermal properties of the TFMG were characterized using DSC. The glass transition temperature, T_g , and crystallization temperature, T_x , of Zr₆₀Cu₂₄Al₁₁Ni₅ TFMG were determined to be 682.9 K (409.9 °C) and 770.6 K (497.6 °C), respectively (see Supplementary Figure S1). The thermal aging of TFMG/TE couples was carried out below T_g to ensure no crystallization occurs. The wide supercooled liquid region ($\Delta T_x = T_x - T_g$) of TFMG implies a higher resistance to the nucleation and growth of crystalline phases upon annealing³¹. After long-term annealing, the TFMG remained well-adhered to the TE surface. The low magnification top-view SEM image of the TFMG/TE sample annealed for 24 hours shows no sign of spallation, buckling or incomplete coverage of the TFMG (Supplementary Figure S2). In addition to high thermal stability, a low electrical contact resistivity (ρ_c) is desirable in TFMG/TE couples. In TE devices, the ρ_c between the TE material and metal electrode is expected to fall in the range of 10^{-9} ($\Omega \text{ m}^2$) to 10^{-8} ($\Omega \text{ m}^2$)³². The ρ_c between the TFMG and TE substrate, obtained using the transmission line measurement (TLM) method (Supplementary Figure S3), clearly satisfies the requirement having a value of 1.62×10^{-9} ($\Omega \text{ m}^2$). The electrical properties, including sheet resistance, resistivity, contact resistance and specific contact resistivity of TFMG/Si, Ni/Si, and TFMG/TE are further summarized in Supplementary Table S1. Typical cross-sectional STEM images, SAED patterns and EDS line-scan results of as-deposited TFMG/TE samples and those annealed at 400 °C for 8–360 h are shown in Fig. 1(a–e). The red arrows in the images indicate the EDS line-scan direction. The corresponding compositional profiles are presented to the right of the images. In the EDS line-scan results, the Zr signal represents the TFMG. The SAED patterns of the TFMG layers are embedded in each micrograph. In Fig. 1(a), the featureless amorphous structure and a typical halo SAED pattern of TFMG is shown in the as-deposited condition. After annealing at 673 K for 8 h there was no indication that IMCs had formed, while a homogeneous diffusion layer with a thickness of ≈ 30 nm was found in the TFMG coating [Fig. 1(b)]. The compositional profile indicates this layer is Se-rich. SAED of the TFMG layer exhibits a halo pattern with minor diffraction-spots, which may be due to oxidation-induced-crystallization in the TFMG upon annealing. After annealing for 48 h [Fig. 1(c)], the width of the Se-rich diffusion layer was found to homogeneously increase to ≈ 110 nm. The Se diffusion layer continued to grow with increasing annealing time. Se atoms were found to have diffused throughout the entire TFMG layer after 120 h [Fig. 1(d)] and 360 h [Fig. 1(e)]. From the SAED pattern, we found that the main phase of the whole TFMG layer remained amorphous after annealing for 8–120 h. This indicates that Se atoms, diffusing into TFMG, do not react with TFMG to form a

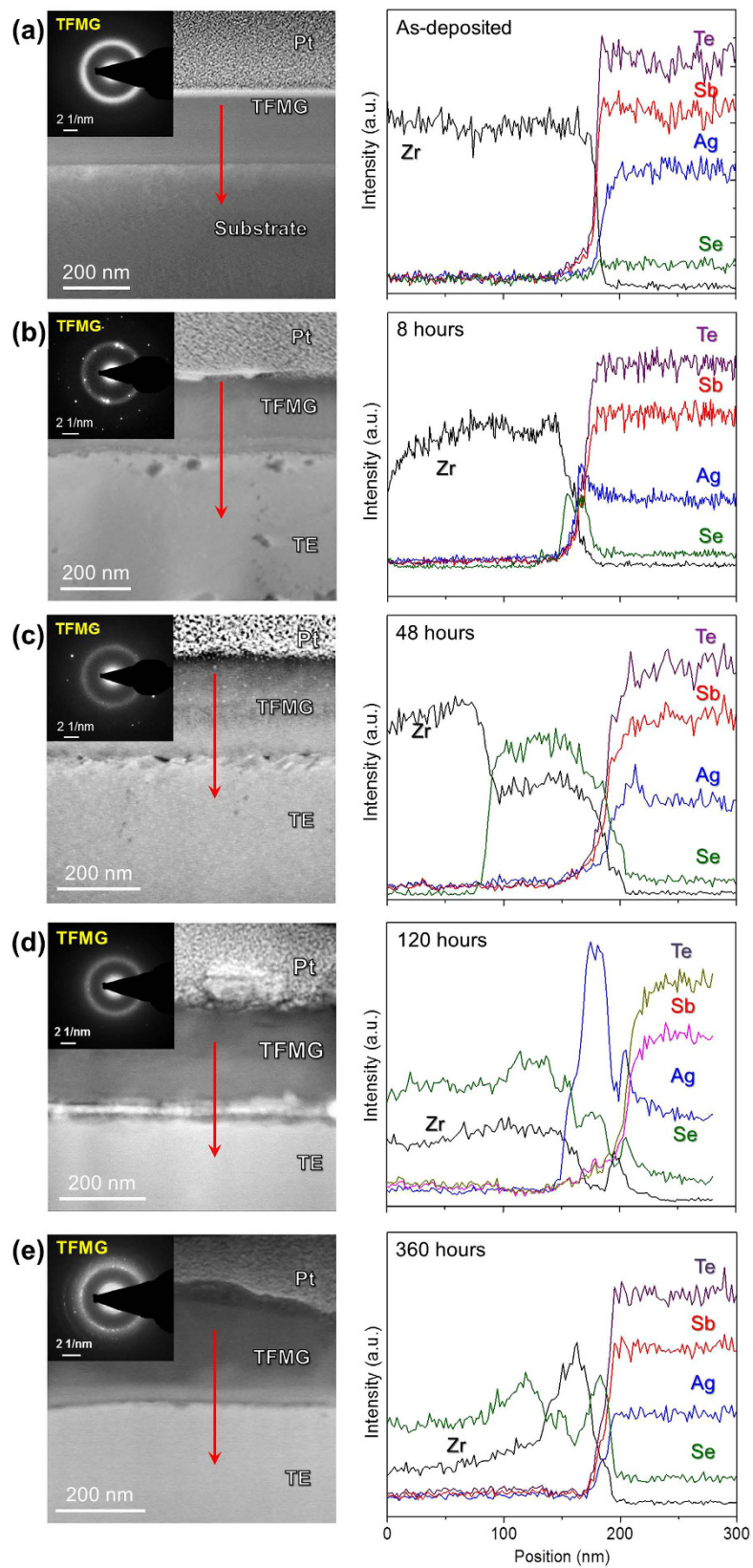


Figure 1. Cross-sectional STEM images together with the elemental line scan results of TFMG/AgSbSe_xTe_{2-x} couples in (a) as-deposited condition and reacted at 673 K for (b) 8 hours, (c) 48 hours (d) 120 hours and (e) 360 hours. All the diffraction patterns embedded in the upper-left corners were obtained from the TFMG layer.

crystalline phase. Additionally, the TFMG layer did not react with the TE substrate to form detrimental IMCs. In brief, for every annealed TFMG/TE sample, there was a well-defined, continuous interface.

The cross-sectional STEM images and EDS line-scan results of as-deposited, 8-, 48-, 120-, and 360-hours-annealed Ni/AgSbSe_xTe_{2-x} samples can be found in Fig. 2(a–e). In the as-deposited condition, the 200 nm thick polycrystalline Ni layer and the clearly defined film/substrate interface were observed [Fig. 2(a)]. The ring SAED pattern obtained from the Ni layer exhibited face-centered cubic structure, as identified from the (111), (200), (220) and (311) planes [see the inset of Fig. 2(a)]. In all annealed samples [Fig. 2(b–e)], the entire Ni layer significantly reacted with the TE substrate to form IMCs. The reaction layer thickness was larger than 500 nm. The SAED patterns, acquired from a single grain in the reaction layer, and EDS investigations suggest that hexagonal NiSb_{1-x}Te_{2x} (0.28 < x < 0.66) is the primary IMC formed from annealing at 673 K. We note that NiSb_{1-x}Te_{2x} is an equilibrium phase reported in the Ni-Te-Sb system at 673 K (400 °C)³³. Due to the variation of grain orientations in the reaction layer, SAED patterns with different zone axes were obtained [see the insets of Fig. 2(b–e)]. Additionally, the pores seen in the images of the Ni/TE samples can be attributed to the preferential etching of more reactive regions at the grain-boundaries of IMCs and at the IMC/TE interface upon FIB milling. Nevertheless, the formation of IMCs in the Ni diffusion barrier can lead to poor mechanical properties at the joint as well as high electrical- and thermal-resistance contacts.

The comparison shown in Fig. 3 visually demonstrates that the Zr-based TFMG acted as an effective diffusion barrier layer even after long-term high-temperature annealing, while the Ni layer did not. The extensive interdiffusion/reaction of Ni, Sb and Te resulted in a wide (>500 nm) interfacial reaction zone comprised of NiSb_{1-x}Te_{2x} intermetallic compounds and cracks, which could lead to electrical or mechanical failure in thermoelectric modules. However, the success of the TFMG as an effective diffusion barrier may be largely attributed to the formation of a homogeneous Se-rich layer at the TFMG/TE interface (Fig. 3(a)). Having a thickness of ≈100 nm after annealing at 400 °C for 48 h, this layer ensures good adhesion between the TFMG and the TE substrate. Additionally, using the Se atom as a tracer species allowed for the study of the diffusional properties of the metallic glass.

Diffusion in metallic glasses has drawn a great amount of attention due to its technological relevance³⁴. Unlike diffusion in crystalline materials, mainly attributed to vacancy and/or interstitial migration triggered by independent random atomic jumps³⁵, the mechanism of diffusion in amorphous glass is generally acknowledged to be a collective hopping process³⁶. This mechanism may be responsible for the homogeneous Se-rich diffusion layer as observed in Fig. 3(b). One of the popular approaches to explain the atomic mobility in MGs is the free-volume model proposed previously by Spaepen³⁷. According to this model, the diffusion defects and flow defects, the so-called free volume, serve as both diffusive and viscous media in amorphous alloys. These free volumes are frozen into the structure upon forming the alloy. Using faster quench rates to fabricate MGs produces more free volume defects, increasing the excess volume of the structure. It was also found that the diffusivity in MGs is correlated with the excess volume present in the as-quenched material³⁴. Below T_g, due to the high quench rate of sputtering deposition³⁸, the TFMG can be viewed as a frozen-in liquid. As such, it has a large amount of homogeneously dispersed free volume. Therefore, the diffusion across the TFMG/TE couple can be simply treated as the one-way diffusion of Se into the TFMG. This may also be expected as Se exhibits the smallest atomic volume among all the elements involved in the TFMG/TE couple. The diffusion of Se can be described by Fick's second law:

$$\frac{\partial C(x, t)}{\partial t} = D \frac{\partial^2 C(x, t)}{\partial x^2} \quad (1)$$

where $C(x, t)$ stands for the chemical concentration of the tracer species at a specific position, x , and time, t , and D represents the diffusion coefficient. Given that the diffusion is semi-infinite, the concentration distribution of the tracer species (e.g. Se) follows the thin-film solution of Fick's second law:

$$C(x, t) = \frac{S_0}{\sqrt{\pi Dt}} e^{-x^2/4Dt} \quad (2)$$

where S_0 refers to the initial concentration of tracer atoms (per unit area) at the surface of the as-deposited thin film. Since the annealing time, t , was predetermined and the distribution of Se could be obtained from the above-mentioned EDS data, the diffusivity (D) of Se was estimated from the slope ($-1/4Dt$) of the logarithmic plot of Eq. (2). Based on the diffusion coefficients reported for various tracer species in metallic glasses³⁴, it is expected that D falls in the range of 10^{-23} (m²/s) to 10^{-16} (m²/s).

Figure 4(a) summarizes the Se diffusion distance from the TFMG/TE interface, as determined by the EDS compositional line-scan, for samples annealed 8–120 h at 400 °C. There is a clear square law dependence of the diffusion distance of Se with increasing annealing time. Additionally, after 120 h, the Se was found to be distributed in the whole 200 nm thick TFMG layer. For comparison, the diffusion distance of Ni, determined in this work, and in p -type (Bi, Sb)₂Te₃ and n -type Bi₂(Se, Te)₃ at 500 K³⁹ are collected in Fig. 4(a). The migration of Ni in crystalline materials is clearly more extensive than that of Se in TFMG. Other determinations about the diffusion of species in crystalline or amorphous materials can be deliberated by comparing the diffusion coefficients in Fig. 4(b).

The diffusion coefficient (D) of Se in the Zr-based TFMG at 673 K, calculated according to Eq. (2), is shown in Fig. 4(b). The D decreases rapidly from $D \approx 6.5 \times 10^{-21}$ (m²/s) after 8 h, to a plateau value of $D \approx 1.2 \times 10^{-24}$ (m²/s), after 120 h annealing. This can be ascribed to the structural relaxation of the TFMG during annealing below T_g, resulting in the annihilation of excess free volume^{40,41}, and thus reducing the diffusivity of Se. In other words, atoms require less energy to hop through the less dense structure (as-deposited condition) than to hop

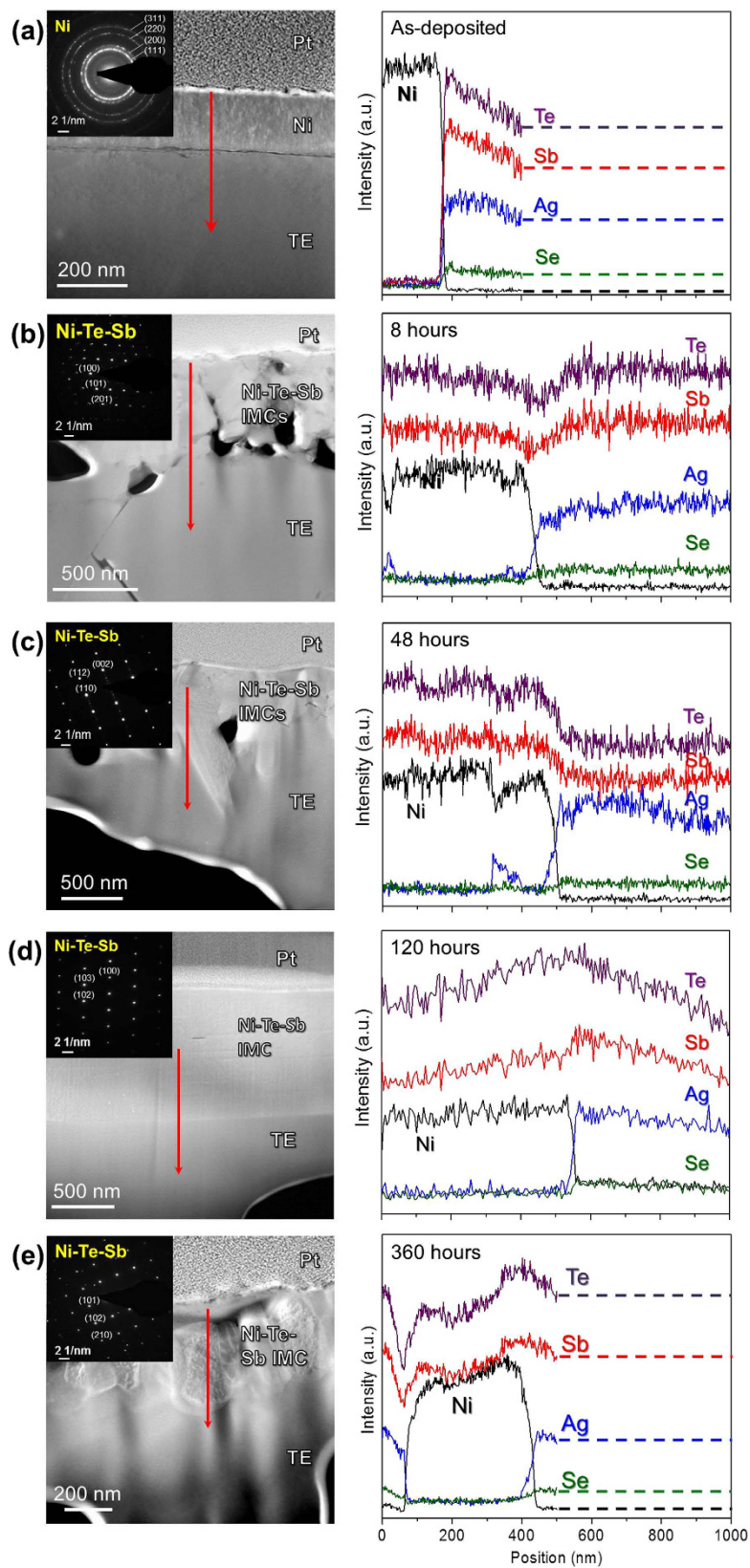


Figure 2. Cross-sectional STEM images together with the elemental line scan results of Ni/AgSbSe_xTe_{2-x} couples in (a) as-deposited condition and reacted at 673 K for (b) 8 hours, (c) 48 hours (d) 120 hours and (e) 360 hours. The diffraction patterns embedded in the upper-left corners were obtained from Ni layer in (a) and Ni-Te-Sb IMCs regions in (b–e).

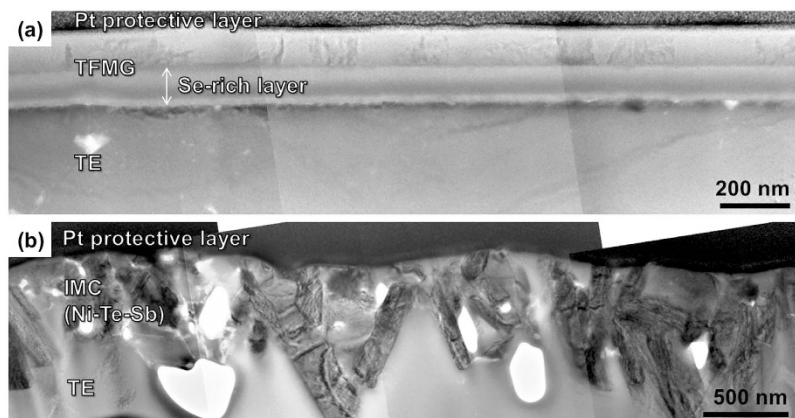


Figure 3. Low magnification bright-field images of (a) TFMG/AgSbSe_xTe_{2-x} and (b) Ni/AgSbSe_xTe_{2-x} couples reacted at 673 K for 48 hours.

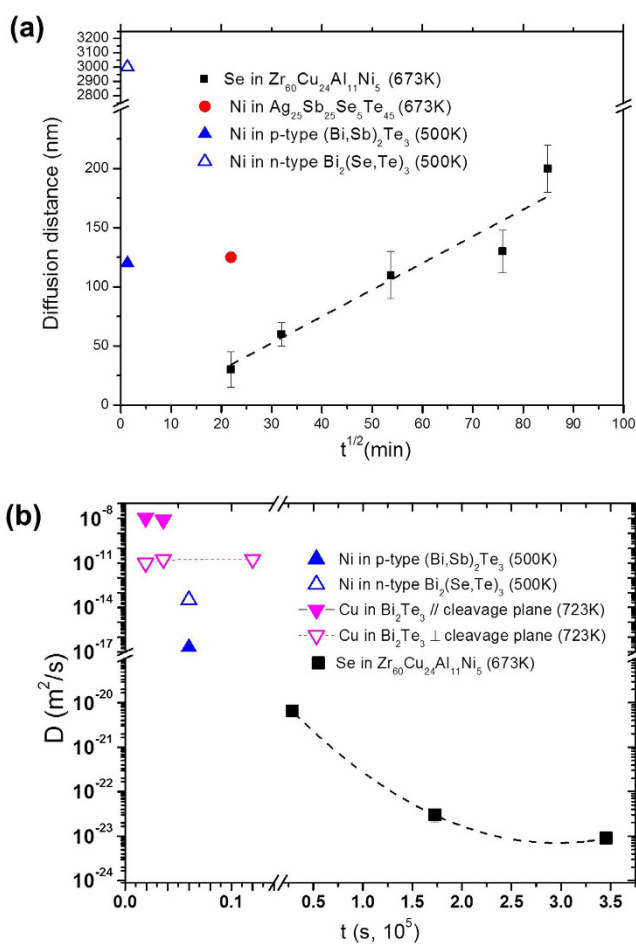


Figure 4. Plots of (a) the diffusion distance of Se in TFMG, Ni in TE substrate, Ni in p-type (Bi, Sb)₂Te₃ and n-type Bi₂(Se, Te)₃[19] vs. the square root of annealing times of 8–120 hours and (b) diffusion coefficient (D) of Se atoms in TFMG, Ni in p-type (Bi, Sb)₂Te₃ and n-type Bi₂(Se, Te)₃[19], Cu in Bi₂Te₃ measured parallel and perpendicular to cleavage planes [36] vs. various annealing time.

through the more dense structure (after annealing). Consequently, the D of Se decreases with increasing annealing time as the structure of the TFMG tends from the as-deposited condition towards the fully relaxed state, at which point D remains constant [Fig. 4(b)].

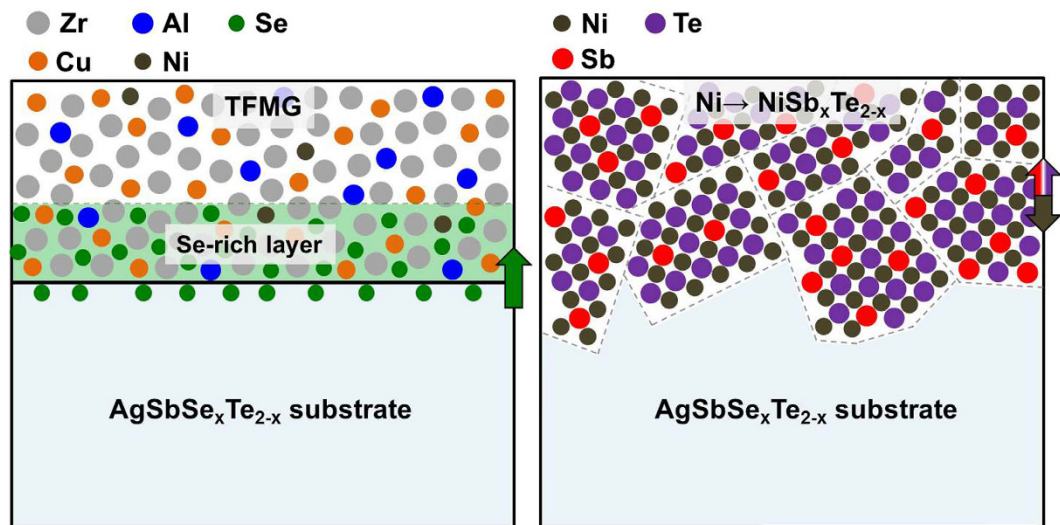


Figure 5. The schematic presentation of the interfacial diffusion of the TFMG/AgSbSe_xTe_{2-x} and the Ni/AgSbSe_xTe_{2-x} reaction couples.

The D of Ni in p -type (Bi, Sb)₂Te₃ and n -type Bi₂(Se, Te)₃ at 500 K³⁹ and that of Cu in Bi₂Te₃ (measured parallel and perpendicular to the cleavage planes)⁴² are presented together in Fig. 4(b). For further comparison, the D of Se in Bi₂Te₃ is on the order of 10^{-15} – 10^{-18} (m²/s)⁴³ at temperatures along the solidus line. The D of Se in amorphous TFMG [$\approx 10^{-20}$ – 10^{-24} (m²/s)] is 10^6 – 10^7 and 10^{12} – 10^{13} times smaller compared with that of Ni in Bi₂Te₃ [10^{-14} (m²/s) – 10^{-17} (m²/s)] and that of Cu in Bi₂Te₃ [10^{-8} (m²/s) – 10^{-11} (m²/s)]. As for the self-diffusion and impurity diffusion coefficients reported for other TFMGs around 673 K ($D \approx 10^{-17}$ – 10^{-23} (m²/s)), as summarized in ref. 30), we find the D of Se to be of the same magnitude, suggesting that the grain-boundary-free structure, effectively prohibits the interdiffusion at the interface of dissimilar materials.

Schematic illustrations of the interfacial diffusion of the TFMG/TE and the Ni/TE reaction couples are presented in Fig. 5. Due to the grain boundary-free structure, Se atoms from the TE substrate diffuse uniformly into the TFMG, via its free-volume, during annealing below T_g . In contrast, the grain boundaries in the Ni layer serve as an atomic diffusion path, resulting in significant interdiffusion and reaction between Ni and the substrate, as to form NiSb_xTe_{2-x} IMCs.

Conclusion

We demonstrate that the Zr-based TFMG with a thin thickness of 200 nm serves as an effective diffusion barrier layer for mid-temperature TE modules using AgSbTe₂ as a substrate. After long-term annealing at 673 K, the TFMG/TE interface reveals no observable IMCs, presumably due to the grain-boundary free structure of the TFMG. Instead, a homogeneous Se-rich diffusion region is located at the TFMG/TE interface, indicating good adhesion between the TFMG and the TE substrate. We also find that the diffusion of Se in TFMG follows Fick's second law while the diffusivity of Se decreases with increasing annealing time, which can be attributed to the annihilation of excess free-volume due to the thermal relaxation of the TFMG. On the other hand, a 200 nm thick Ni layer severely reacts with the TE substrate, under identical annealing conditions, and forms NiSb_xTe_{2-x} IMCs. As IMCs can be detrimental to the performance of TE modules, the Zr-based TFMG, possessing high strength, high thermal stability and low electrical contact resistivity, shows great potential as an alternative diffusion barrier layer for mid-temperature TE modules.

Methods

The polycrystalline, quaternary Ag₂₅Sb₂₅Se₅Te₄₅ alloy, exhibiting $zT \approx 1.4$ at 673 K²⁴, was synthesized by unidirectional solidification in a Bridgman furnace. Details of the Bridgman method have been reported previously²⁴. In short, five grams of homogenized Ag₂₅Sb₂₅Se₅Te₄₅ were loaded in a 7 mm × 9 mm quartz tube, sealed under vacuum and placed in a Bridgman furnace. The three heating zones created a large temperature gradient (50 K/mm) along the axial direction. At first, the ampoule was placed in the high-temperature zone at a temperature above the melting point of the TE alloy (≈ 1123 K) for at least 1 h, to ensure homogenized melting. Unidirectional solidification was achieved as the ampoule moved gradually downward, at a rate of 5 mm/h, from the high-temperature zone (≈ 1123 K) to the low-temperature zone (≈ 300 K). The Bridgman-grown Ag₂₅Sb₂₅Se₅Te₄₅ was then cut into ~ 1 mm thick pellets, grinded using a series of SiC sand papers (800–2400 grit), and then polished using Al₂O₃ suspension with gradually reduced particle sizes from 1 to 0.05 μ m, for the subsequent thin-film deposition process.

Zr₆₀Cu₂₄Al₁₁Ni₅ (at%) TFMG and pure Ni (99.99%) were deposited on two different sides of the Ag₂₅Sb₂₅Se₅Te₄₅ substrate by radio-frequency magnetron sputtering with no external heating. Zr₅₅Cu₂₉Al₁₁Ni₅ alloy and pure Ni sputtering targets were used in a vacuum system with a base pressure of $< 1 \times 10^{-6}$ Torr. The Ar sputtering pressure was 3 mTorr and a -20 V bias was applied to the substrates for both depositions. After the

thin-film depositions, the reaction couple of TFMG/Ag₂₅Sb₂₅Se₅Te₄₅ (TE substrate)/Ni was again sealed under vacuum and placed in a 673 K furnace for various lengths of time (*i.e.*, 8, 48, 120 and 360 hours).

The sheet resistance and the resistivity were measured using a resistivity meter (Loresta-AX MCP-T370). The contact resistance and specific contact resistance of as-deposited TFMG/TE sample was assessed based on a transmission line measurement⁴⁴ (TLM) technique with the semiconductor parameter analyzer (Agilent B1500A) at room temperature. The TFMG contacts with length of 150 μm and width of 600 μm were deposited on the TE substrate using a shadow mask. The contacts were spaced from 250 to 2000 μm apart. The current (I) and the voltage (V) were measured on the differently spaced contact electrodes and the resistance (R) was determined from the inverse slope of a linear fit of the I-V plot.

The thermal properties of the TFMG were characterized using differential scanning calorimetry (DSC, Netzsch 404 F3 Pegasus) from 573 to 973 K (300–700 °C) at a heating rate of 40 K/min under Ar atmosphere. The TFMG layer and TE substrate compositions were determined by energy-dispersive X-ray spectroscopy (EDS) in a scanning electron microscope (SEM), which is part of a dual-beam focused-ion-beam system (FIB, FEI Quanta 3D FEG). Transmission electron microscopy (TEM) sample foils were produced by FIB thinning using 30 kV Ga⁺ beams initially and 5 kV for the final polishing. Prior to FIB thinning, platinum was deposited on top of the samples to protect the thin film-layers from ion-damage. TFMG/TE and Ni/TE microstructures were analyzed by TEM in a FEI TecnaiTM G2 F-20 instrument operated at 200 kV. Selected-area electron diffraction (SAED) with a captured diameter of 200 nm was employed to characterize the structure of local regions in the annealed samples. High-angle annular dark-field (HAADF) imaging and EDS in scanning TEM (STEM) mode were used to acquire the compositional profile across each interface.

References

- Chen, G., Dresselhaus, M. S., Dresselhaus, G., Fleurial, J. P. & Caillat, T. Recent developments in thermoelectric materials. *International Materials Reviews* **48**, 45–66, doi: 10.1179/095066003225010182 (2003).
- Snyder, G. J. & Toberer, E. S. Complex thermoelectric materials. *Nature Materials* **7**, 105–114, doi: 10.1038/nmat2090 (2008).
- He, W. *et al.* Recent development and application of thermoelectric generator and cooler. *Applied Energy* **143**, 1–25, doi: 10.1016/j.apenergy.2014.12.075 (2015).
- Yang, L., Chen, Z. G., Hong, M., Han, G. & Zou, J. Enhanced Thermoelectric Performance of Nanostructured Bi₂Te₃ through Significant Phonon Scattering. *ACS Applied Materials and Interfaces* **7**, 23694–23699, doi: 10.1021/acsami.5b07596 (2015).
- Pei, Y., Lensch-Falk, J., Toberer, E. S., Medlin, D. L. & Snyder, G. J. High thermoelectric performance in PbTe due to large nanoscale Ag₂Te precipitates and la doping. *Advanced Functional Materials* **21**, 241–249, doi: 10.1002/adfm.201000878 (2011).
- Ikeda, T., Ravi, V. A. & Snyder, G. J. Formation of Sb₂Te₃ Widmanstätten precipitates in thermoelectric PbTe. *Acta Materialia* **57**, 666–672, doi: 10.1016/j.actamat.2008.10.005 (2009).
- Singh, N. K. *et al.* The effect of doping on thermoelectric performance of p-type SnSe: Promising thermoelectric material. *Journal of Alloys and Compounds* **668**, 152–158, doi: http://dx.doi.org/10.1016/j.jallcom.2016.01.190 (2016).
- Xia, H. *et al.* Bonding and high-temperature reliability of NiFeMo alloy/n-type PbTe joints for thermoelectric module applications. *Journal of Materials Science* **50**, 2700–2708, doi: 10.1007/s10853-015-8820-8 (2015).
- Li, C. C. *et al.* Interfacial reactions between PbTe-based thermoelectric materials and Cu and Ag bonding materials. *Journal of Materials Chemistry C* **3**, 10590–10596, doi: 10.1039/c5tc01662b (2015).
- Li, C. C. *et al.* Silver as a highly effective bonding layer for lead telluride thermoelectric modules assembled by rapid hot-pressing. *Energy Conversion and Management* **98**, 134–137, doi: 10.1016/j.enconman.2015.03.089 (2015).
- Chen, W. A. *et al.* Interfacial reactions in Ni/CoSb₃ couples at 450 °C. *Journal of Alloys and Compounds* **632**, 500–504, doi: 10.1016/j.jallcom.2015.01.176 (2015).
- Xia, H. *et al.* Interfacial reaction between Nb foil and n-type PbTe thermoelectric materials during thermoelectric contact fabrication. *Journal of Elec Materi* **43**, 4064–4069, doi: 10.1007/s11664-014-3350-8 (2014).
- Xia, H., Drymiotis, F., Chen, C. L., Wu, A. & Snyder, G. J. Bonding and interfacial reaction between Ni foil and n-type PbTe thermoelectric materials for thermoelectric module applications. *Journal of Materials Science* **49**, 1716–1723, doi: 10.1007/s10853-013-7857-9 (2014).
- Poudel, B. *et al.* High-thermoelectric performance of nanostructured bismuth antimony telluride bulk alloys. *Science* **320**, 634–638, doi: 10.1126/science.1156446 (2008).
- Zhang, H., Jing, H. Y., Han, Y. D., Xu, L. Y. & Lu, G. Q. Interfacial reaction between n- and p-type thermoelectric materials and SAC305 solders. *Journal of Alloys and Compounds* **576**, 424–431, doi: 10.1016/j.jallcom.2013.05.129 (2013).
- Chuang, C.-H., Lin, Y.-C. & Lin, C.-W. Intermetallic Reactions during the Solid-Liquid Interdiffusion Bonding of Bi₂Te_{2.55}Se_{0.45} Thermoelectric Material with Cu Electrodes Using a Sn Interlayer. *Metals* **6**, doi: 10.3390/met6040092 (2016).
- Cook Iii, G. O. & Sorensen, C. D. Overview of transient liquid phase and partial transient liquid phase bonding. *Journal of Materials Science* **46**, 5305–5323, doi: 10.1007/s10853-011-5561-1 (2011).
- Zybala, R., Wojciechowski, K., Schmidt, M. & Mania, R. Junctions and diffusion barriers for high temperature thermoelectric modules. *Materiały Ceramiczne* **62**, 481–485 (2010).
- Wojciechowski, K. T., Zybala, R. & Mania, R. High temperature CoSb₃-Cu junctions. *Microelectronics Reliability* **51**, 1198–1202, doi: http://dx.doi.org/10.1016/j.microrel.2011.03.033 (2011).
- Zhao, D., Li, X., He, L., Jiang, W. & Chen, L. Interfacial evolution behavior and reliability evaluation of CoSb₃Ti/Mo-Cu thermoelectric joints during accelerated thermal aging. *Journal of Alloys and Compounds* **477**, 425–431, doi: 10.1016/j.jallcom.2008.10.037 (2009).
- Zhao, D., Li, X., He, L., Jiang, W. & Chen, L. High temperature reliability evaluation of CoSb₃/electrode thermoelectric joints. *Intermetallics* **17**, 136–141, doi: 10.1016/j.intermet.2008.10.010 (2009).
- Gu, M. *et al.* Study on the interfacial stability of p-type Ti/CyFexCo_{4-x}Sb₁₂ thermoelectric joints at high temperature. *Journal of Alloys and Compounds* **671**, 238–244, doi: http://dx.doi.org/10.1016/j.jallcom.2016.02.041 (2016).
- Song, B. *et al.* The effects of diffusion barrier layers on the microstructural and electrical properties in CoSb₃ thermoelectric modules. *Journal of Alloys and Compounds* **617**, 160–162, doi: http://dx.doi.org/10.1016/j.jallcom.2014.07.066 (2014).
- Wu, H. J. *et al.* State of the art Ag_{50-x}Sb_xSe_{50-y}Te_y alloys: Their high zT values, microstructures and related phase equilibria. *Acta Materialia* **93**, 38–45, doi: 10.1016/j.actamat.2015.04.011 (2015).
- Chu, J. P. *et al.* Thin film metallic glasses: Unique properties and potential applications. *Thin Solid Films* **520**, 5097–5122, doi: http://dx.doi.org/10.1016/j.tsf.2012.03.092 (2012).
- Wang, C.-W., Yiu, P., Chu, J. P., Shek, C.-H. & Hsueh, C.-H. Zr-Ti-Ni thin film metallic glass as a diffusion barrier between copper and silicon. *Journal of Materials Science* **50**, 2085–2092, doi: 10.1007/s10853-014-8770-6 (2015).
- Wahyu, D., Lingjun, X., Tai-Nan, L., Chia-wen, C. & Jinn, P. C. Thin film metallic glass as a diffusion barrier for copper indium gallium selenide solar cell on stainless steel substrate: A feasibility study. *Japanese Journal of Applied Physics* **55**, 080303 (2016).

28. Diyatmika, W., Chu, J. P., Yen, Y. W. & Hsueh, C. H. Sn whisker mitigation by a thin metallic-glass underlayer in Cu-Sn. *Applied Physics Letters* **103**, 241912, doi: <http://dx.doi.org/10.1063/1.4847336> (2013).
29. Yamasaki, M., Kagao, S. & Kawamura, Y. Thermal diffusivity and conductivity of Zr₅₅Al₁₀Ni₅Cu₃₀ bulk metallic glass. *Scripta Materialia* **53**, 63–67, doi: <http://dx.doi.org/10.1016/j.scriptamat.2005.03.021> (2005).
30. Yoon, J. W., Kim, S. W., Koo, J. A. M., Kim, D. G. & Jung, S. B. Reliability investigation and interfacial reaction of ball-grid-array packages using the lead-free Sn-Cu solder. *Journal of Elec Materi* **33**, 1190–1199 (2004).
31. Zhang, A., Chen, D. & Chen, Z. Predicting the thermal stability of RE-based bulk metallic glasses. *Intermetallics* **18**, 74–76, doi: <http://dx.doi.org/10.1016/j.intermet.2009.06.009> (2010).
32. da Silva, L. W. & Kaviani, M. Micro-thermoelectric cooler: interfacial effects on thermal and electrical transport. *International Journal of Heat and Mass Transfer* **47**, 2417–2435, doi: <http://dx.doi.org/10.1016/j.ijheatmasstransfer.2003.11.024> (2004).
33. Laufek, F., Drábek, M. & Skála, R. The system Ni-Sb-Te at 400°C. *Canadian Mineralogist* **48**, 1069–1079, doi: 10.3749/canmin.48.5.1069 (2010).
34. Faupel, F. *et al.* Diffusion in metallic glasses and supercooled melts. *Reviews of Modern Physics* **75**, 237–280 (2003).
35. Greer, A. L. Through a glass, lightly. *Nature* **402**, 132–133, doi: 10.1038/45946 (1999).
36. Zöllmer, V., Rätzke, K., Faupel, F. & Meyer, A. Diffusion in a metallic melt at the critical temperature of mode coupling theory. *Physical Review Letters* **90** (2003).
37. Spaepen, F. A microscopic mechanism for steady state inhomogeneous flow in metallic glasses. *Acta Metallurgica* **25**, 407–415, doi: [http://dx.doi.org/10.1016/0001-6160\(77\)90232-2](http://dx.doi.org/10.1016/0001-6160(77)90232-2) (1977).
38. Barbee, T. W., Holmes, W. H., Keith, D. L., Pyzyna, M. K. & Ilonca, G. Synthesis of amorphous niobium-nickel alloys by vapor quenching. *Thin Solid Films* **45**, 591–599, doi: [http://dx.doi.org/10.1016/0040-6090\(77\)90251-6](http://dx.doi.org/10.1016/0040-6090(77)90251-6) (1977).
39. Lan, Y. C., Wang, D. Z., Chen, G. & Ren, Z. F. Diffusion of nickel and tin in p-type (Bi, Sb)₂Te₃ and n-type Bi₂(Te, Se)₃ thermoelectric materials. *Applied Physics Letters* **92**, doi: 10.1063/1.2896310 (2008).
40. Haruyama, O. & Inoue, A. Free volume kinetics during sub-T_g structural relaxation of a bulk Pd₄₀Ni₄₀P₂₀ metallic glass. *Applied Physics Letters* **88**, 131906, doi: <http://dx.doi.org/10.1063/1.2189833> (2006).
41. Slipenyuk, A. & Eckert, J. Correlation between enthalpy change and free volume reduction during structural relaxation of Zr₅₅Cu₃₀Al₁₀Ni₅ metallic glass. *Scripta Materialia* **50**, 39–44, doi: <http://dx.doi.org/10.1016/j.scriptamat.2003.09.038> (2004).
42. Carlson, R. O. Anisotropic diffusion of copper into bismuth telluride. *Journal of Physics and Chemistry of Solids* **13**, 65–70 (1960).
43. Chitroub, M., Scherrer, S. & Scherrer, H. Anisotropy of the selenium diffusion coefficient in bismuth telluride. *Journal of Physics and Chemistry of Solids* **61**, 1693–1701, doi: [http://dx.doi.org/10.1016/S0022-3697\(00\)00031-7](http://dx.doi.org/10.1016/S0022-3697(00)00031-7) (2000).
44. Reeves, G. K. & Harrison, H. B. Obtaining the Specific Contact Resistance from Transmission Line Model Measurements. *IEEE Electron Device Letters* **3**, 111–113, doi: 10.1109/EDL.1982.25502 (1982).

Acknowledgements

The authors acknowledge the financial support of Ministry of Science and Technology of Taiwan (MOST 103-2218-E-110-007-MY2 & 104-2218-E-011-018). Part of this work was supported by NASA's Science Mission Directorate under the Radioisotope Power Systems Thermoelectric Technology Development Project.

Author Contributions

J.P.C., C.-C.Y. and H.J.W. conceived the experimental design. C.C.Y., P.-Y.D. and H.-J.W. conducted the experiments and analyzed the results. All authors discussed and commented on the manuscript.

Additional Information

Supplementary information accompanies this paper at <http://www.nature.com/srep>

Competing Interests: The authors declare no competing financial interests.

How to cite this article: Yu, C.-C. *et al.* Thin-film metallic glass: an effective diffusion barrier for Se-doped AgSbTe₂ thermoelectric modules. *Sci. Rep.* **7**, 45177; doi: 10.1038/srep45177 (2017).

Publisher's note: Springer Nature remains neutral with regard to jurisdictional claims in published maps and institutional affiliations.



This work is licensed under a Creative Commons Attribution 4.0 International License. The images or other third party material in this article are included in the article's Creative Commons license, unless indicated otherwise in the credit line; if the material is not included under the Creative Commons license, users will need to obtain permission from the license holder to reproduce the material. To view a copy of this license, visit <http://creativecommons.org/licenses/by/4.0/>

© The Author(s) 2017